On Convergence Performance of Discrete-Time Optimal Control Based Tracking Differentiator

Journal:	*Transactions on Industrial Electronics*
Manuscript ID	Draft
Manuscript Type:	Regular paper
Manuscript Subject:	Control and Signal Processing
Keywords:	tracking differentiator, active disturbance rejection control, Control engineering
Are any of authors IEEE Member?:	Yes
Are any of authors IES Member?:	No

SCHOLARONE™
Manuscripts

On Convergence Performance of Discrete-Time Optimal Control Based Tracking Differentiator

Abstract—**Time optimal control (TOC) based tracking differentiator (TD) was first proposed by Han [1] as a practical solution to avoid setpoint jump in active disturbance rejection control (ADRC). In practice, the discrete-time optimal control (DTOC) is implemented in the form of state feedback for a double-integral system, which is widely used to design controllers, observers and noise-tolerant differentiators. The convergence of the DTOC-TD, however, has not been fully understood. This paper provides a rigorous full convergence analysis of the DTOC-TD. It then illustrates the frequency-domain characteristics, showing that the performances of this DTOC-TD in signal-tracking filtering and differentiation acquisition approximate a low-pass filter and a bandpass filter, respectively. Finally, the case studies including comparison simulations and experiments on processing gap sensor' signals in the suspension system of maglev train are carried out to verify the effectiveness of the DTOC-TD.**

Index Terms—**Convergence, discrete-time optimal control, tracking differentiator, filtering, differentiation, frequency-domain characteristics, maglev train.**

I. INTRODUCTION

THE real-time differentiation estimation of signals is commonly used in the feedback control, the fault detection and isolation and many other fields [1]- [3]. Extensive studies have been carried out to design exact differentiators such as the super-twisting algorithm based robust exact differentiator [4], [5], the high-gain observer-based differentiator [6], the linear time-derivative tracker [7] and so forth [8], [9]. Time optimal control (TOC) based tracking differentiator (TD), first proposed by Jinqing Han [1], serves not only a transient profile that the system output can reasonably follow to avoid setpoint jump in active disturbance rejection control (ADRC), but also the differentiation acquisition from noise-polluted and/or discontinuous signals [10]- [12].

The applications of TOC solution, the bang-bang control, however, are quite limited because there exists frequent switching of the control signals between two extreme values around the switching curve, particularly around the origin [13], [14]. This may lead to excessive wear and tear of the actuators [15]. On the other hand, with the developments in computer control technology, most control algorithms are now implemented in the discrete-time domain. These lead to the discrete-time optimal control (DTOC), denoted as $fhan$, based TD for practical implementations [1], [16]. This TD sets a weaker condition on the stability of the systems to be constructed. Also, this noise-tolerant TD has advantageous smoothness compared with the chattering and over-shoot problems encountered by sliding-mode-based differentiators [17]- [19]. The advantage of the chattering alleviation comes from the adoption of a boundary level around the switching curve in the $fhan$ algorithm.

This closed-form $fhan$ algorithm was derived for a discrete-time, double-integral system using the method of isochronic regions; it demonstrates that the solution for DTOC problem is not necessarily a bang-bang control [1], [20]. Also, instead of chattering, the DTOC can produce a smooth control signal that results in the performance similar to that of the bang-bang control. As verified in various simulation results, the $fhan$ algorithm is convergent and fast [21]- [23]. However, the rigorous full convergence proof of this DTOC-TD has not been done. In this paper, the convergence of this DTOC-TD is analysed by some easily checkable procedures based on Lyapunov functions. In particular, the state convergence trajectories driven by the corresponding DTOC in different isochronic regions are presented. The characteristics' analysis of this DTOC-TD in frequency domain is given to show that the performances of this DTOC-TD in signal-tracking filtering and differentiation acquisition approximate a low-pass filter and a bandpass filter, respectively. Meanwhile, a rule of thumb for the parameter selection and tuning is proposed to achieve fast convergence. The comparison simulation results are presented to demonstrate its advantages in filtering and differentiation acquisition.

In addition to numerical simulations, the experiments of gap signals processing in maglev train via the DTOC-TD are carried out. For a maglev train, the active suspension control is of high importance to ensure the stability of levitation. To realize such control, it is necessary to obtain sufficient and effective signals reflecting the speed of a suspension electromagnet to participate in designing the feedback controller. In the experiments, we adopt the TD in filtering the gap signals and acquiring speed signals.

The paper is organized as follows: the construction of the DTOC algorithm is presented in Section II. The analysis on the convergence of the DTOC-TD is shown in Section III. In Section IV, the frequency-domain characteristics of the DTOC-TD are analysed. The comparison simulation results and experiments are carried out to demonstrate that this TD has advantages over the existing ones in filtering and differentiation acquisition in Section V, followed by concluding remarks in Section VI.

II. THE DTOC ALGORITHM

In this section, for integrity of the work, the construction of the DTOC algorithm, that is, $fhan$ algorithm [1], is presented by adopting three boundary curves (Γ_A, Γ_B and Γ_C).

Consider a discrete-time double-integral system

$$x(k+1) = Ax(k) + Bu(k), |u(k)| \leq r \qquad (1)$$

where $A = \begin{bmatrix} 1 & h \\ 0 & 1 \end{bmatrix}$, $B = \begin{bmatrix} 0 \\ h \end{bmatrix}$ and $x(k) = [x_1(k), x_2(k)]^T$. The objective here is to derive a TOC algorithm directly in discrete-time domain. This problem is defined as follows.

Definition 1: Given system (1) and its initial state $x(0)$, determine the control signal sequence, $u(0)$, $u(1)$,..., $u(k)$, such that the state $x(k)$ is driven back to the origin in a minimum and finite number of steps, subject to the constraint that $|u(k)| \leq r$. That is, finding $u(k^*)$, $|u(k)| \leq r$, such that $k^* = \min\{k|x(k) = 0\}$.

The method of the isochronic region $(G(k))$ is applied in the deduction of this algorithm. $G(k)$ denotes the set of states that, for any $x(0) \in G(k)$, there is as least one admissible control sequence, $u(0)$, $u(1)$, ..., $u(k)$, which makes the solution of (1) satisfy $x(k) = 0$. This process is divided into two tasks:

I: Determine $G(k)$, i.e., the presentation of the initial condition, $x(0)$, in terms of h and r, from which the state can be driven back to the origin in k steps;

II: For any given initial condition $x(0)$, find the corresponding control signal sequence.

First, let's examine $G(k)$. For any initial state sequence, at least one admissible control sequence exists, e.g., $u(0)$, $u(1)$, ..., $u(k)$, that makes the solution to (1) satisfy $x(k) = 0$. Under the initial condition $x(0)$, the solution is

$$x(k) = A^k x(0) + \sum_{i=1}^{k} A^{k-i} B u(i-1) \qquad (2)$$

Setting $x(k) = 0$ and solving for $x(0)$, we have

$$x(0) = \sum_{i=1}^{k} \begin{bmatrix} ih^2 \\ -h \end{bmatrix} u(i-1) \qquad (3)$$

Then, we have

$$G(k) = \left\{ \sum_{i=1}^{k} \begin{bmatrix} ih^2 \\ -h \end{bmatrix} u(i-1), |u(i)| \leq r \right\} \qquad (4)$$

Consider

$$G(1) = \left\{ \begin{bmatrix} h^2 \\ -h \end{bmatrix} u(0) \right\}$$

$$G(2) = \left\{ \begin{bmatrix} h^2 \\ -h \end{bmatrix} u(0) + \begin{bmatrix} 2h^2 \\ -h \end{bmatrix} u(1) \right\}$$

Let $u(i)$ takes the extreme values of r or $-r$, the resulting $G(k)$, $k = 1, 2$ is plotted on the phase plane (see Fig. 1). Note that $G(1)$ is a straight line between

$$\left\{ a_{-1} = \begin{bmatrix} -h^2 r \\ hr \end{bmatrix}, a_1 = \begin{bmatrix} h^2 r \\ -hr \end{bmatrix} \right\},$$

and $G(2)$ is a parallelogram defined by the four points of

$$\left\{ a_2 = \begin{bmatrix} 3h^2 r \\ -2hr \end{bmatrix}, a_{-2} = \begin{bmatrix} -3h^2 r \\ 2hr \end{bmatrix} \right\}$$

and

$$\left\{ b_2 = \begin{bmatrix} -h^2 r \\ 0 \end{bmatrix}, b_{-2} = \begin{bmatrix} h^2 r \\ 0 \end{bmatrix} \right\}$$
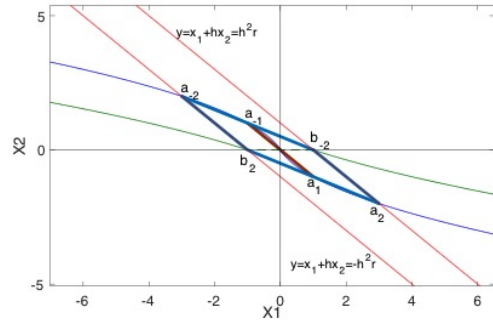

Fig. 1. Isochronic Regions $G(1)$ and $G(2)$ on the phase plane

Let

$$y = x_1 + hx_2 \qquad (5)$$

The boundaries of $G(2)$ are two pairs of parallel lines described as $y = x_1 + hx_2 = \pm h^2 r$ and $y + hx_2 = \pm h^2 r$, respectively. The states of $G(2)$ can be described as

$$\Omega_0 = \{(x_1, x_2) : |y| \leq h^2 r \cap |y + hx_2| \leq h^2 r\}$$

Let

$$a_k = \left\{ \sum_{i=1}^{k} \begin{bmatrix} ih^2 \\ -h \end{bmatrix} u(i-1), u(i) = r \right\}$$

$$a_{-k} = \left\{ \sum_{i=1}^{k} \begin{bmatrix} ih^2 \\ -h \end{bmatrix} u(i-1), u(i) = -r \right\}$$

$$b_k = \left\{ \sum_{i=1}^{k} \begin{bmatrix} ih^2 \\ -h \end{bmatrix} u(i-1), u(0) = r, u(i) = -r \ for \ i > 0 \right\}$$

$$b_{-k} = \left\{ \sum_{i=1}^{k} \begin{bmatrix} ih^2 \\ -h \end{bmatrix} u(i-1), u(0) = -r, u(i) = r \ for \ i > 0 \right\}$$

Clearly, $a_k(a_{-k})$ are initial conditions from which the state is driven back to the origin by using $u(i) = r$ $(u(i) = -r)$, $i = 0, ..., k-1$; furthermore, the broken line connecting $\{a_k, a_{k-1}, ..., a_1, 0\}$ $(\{a_{-k}, a_{-(k-1)}, ..., a_{-1}, 0\})$ is the minimum time state trajectory corresponding to $u(i) = r(u(i) = -r)$, $i = 0, ..., k-1$. According to (3) and the control sequence taken above, we can get the minimum time state trajectory, denoted as Γ_A, as follows:

$$\Gamma_A : x_1 + \frac{x_2|x_2|}{2r} + \frac{1}{2}hx_2 = 0 \qquad (6)$$

where $\Gamma_A = \Gamma_A^+ \cup \Gamma_A^-$ (see Fig. 2). This state trajectory curve overlaps the above broken line at the point $\{a_k, a_{-k}\}$.

The $b_{-k}(b_k)$, $k \geq 2$ are initial conditions from which the state is first driven back to $a_{k-1}(a_{-(k-1)})$ by using $u(0) = -r$ $(u(0) = r)$, and then forced to the origin by using $u(i) = r$ $(u(i) = -r)$, $i = 1, ..., k-1$. Connecting $\{b_{-2}, ..., b_{-(k-1)}, b_{-k}, ...\}$ and $\{..., b_k, b_{k-1}, ..., b_2\}$ forms a broken line. We can get its corresponding curve's expression, denoted as Γ_B, as follows:

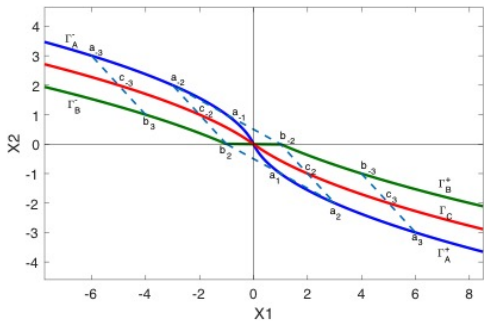$$\Gamma_B : x_1 - s\frac{x_2^2}{2r} + \frac{5}{2}hx_2 - sh^2 r = 0 \qquad (7)$$

Fig. 2. Illustration of Γ_A, Γ_B and Γ_C, where $\Gamma_A = \Gamma_A^+ \cup \Gamma_A^-$, $\Gamma_B = \Gamma_B^+ \cup \Gamma_B^-$

Fig. 3. Illustration of $\tilde{\Gamma}^+$, $\tilde{\Gamma}^-$ and $\tilde{\Gamma}^0$

where $s = \mathrm{sign}(x_1 + hx_2)$ and $\Gamma_B = \Gamma_B^+ \cup \Gamma_B^-$ (see Fig. 2). This curve overlaps the corresponding broken line at the point $\{b_k, b_{-k}, k \geq 2\}$.

Note that, the segments $[b_{-k}a_k]$ ($[b_k a_{-k}]$) are all parallel to each other and their midpoints, c_k (c_{-k}), are initial conditions from which the state is first driven back to a_{k-1} ($a_{-(k_1)}$) by using $u(0) = 0$, and then be forced to the origin by using $u(i) = r$ ($u(i) = -r$), $i = 1, ..., k-1$. This broken line is denoted as Γ^0. Also, we can get its corresponding curve's expression, denoted as Γ_C (see Fig. 2), as follow:

$$\Gamma_C : x_1 + \frac{x_2|x_2|}{2r} + \frac{3}{2}hx_2 = 0 \qquad (8)$$

Connecting the points $\{..., a_k, a_{k-1}, ..., a_2, b_2, ..., b_{k-1}, b_k\}$ forms a boundary denoted as Γ^+, and the points $\{..., b_{-k}, b_{-(k-1)}, ..., b_{-2}, a_{-2}, ..., a_{-(k-1)}, a_{-k}, ...\}$ as Γ^-. Combining functions of Γ_A and Γ_B and the boundary transformation in (5), we have

$$T(x_1, x_2, r, h) = x_2 + \frac{1}{2}(\sqrt{h^2r^2 + 8r|y|} - hr)\mathrm{sign}(y), |y| \geq h^2r \qquad (9)$$

Then $T(x_1, x_2, r, h) = -hr$ corresponds to the parabolas connecting a_k and b_k, respectively, and this curve, denoted as $\tilde{\Gamma}^+$, overlaps Γ^+ at the points $a_k, b_k, k \geq 2$. Similarly, $T(x_1, x_2, r, h) = hr$ corresponds to the parabolas connecting a_{-k} and b_{-k}, respectively, and this curve, denoted as $\tilde{\Gamma}^-$, overlaps Γ^- at the points $a_{-k}, b_{-k}, k \geq 2$. It can also be shown that $T(x_1, x_2, r, h) = 0$ represents $\tilde{\Gamma}^0$, which overlaps Γ^0 at the points $c_{-k}, c_k, k \geq 2$. Moreover, $\tilde{\Gamma}^+$ and $\tilde{\Gamma}^-$ partition the phase plane in a manner of

$$\begin{cases} T(x_1, x_2, r, h) \leq -hr, x = [x_1, x_2]^T is\ below\ \tilde{\Gamma}^+ \\ T(x_1, x_2, r, h) \geq hr, x = [x_1, x_2]^T is\ above\ \tilde{\Gamma}^- \\ T(x_1, x_2, r, h) \leq hr, x = [x_1, x_2]^T is\ between\ \tilde{\Gamma}^+ and\ \tilde{\Gamma}^- \end{cases} \qquad (10)$$

Up to now, any initial condition on the $x_1 - x_2$ plane can be divided into four parts, they are, $G(1)$, $G(2)$, the initial condition ($|y| \geq h^2r$) inside the area bounded by $\tilde{\Gamma}^+$ and $\tilde{\Gamma}^-$ and the rest part (see Fig. 3).

According to the references [1], [20], the complete DTOC algorithm for any initial condition on the $x_1 - x_2$ plane is
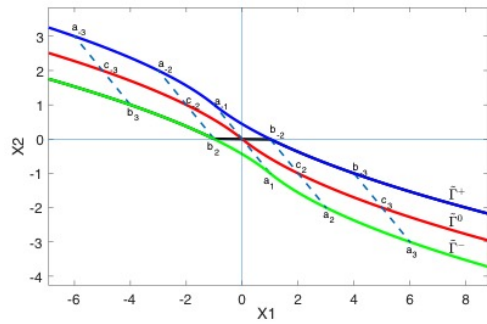
$$u = -r\mathrm{sat}(T(x_1, x_2, r, h), hr) \qquad (11)$$

where

$$T(x_1, x_2, r, h) = \begin{cases} x_2 + \frac{(\sqrt{h^2r^2 + 8r|y|} - hr)}{2}\mathrm{sign}(y), |y| > h^2r \\ x_2 + y/h, |y| \leq h^2r \end{cases} \qquad (12)$$

This algorithm can be coded in a digital computer as in (13).

$$\begin{cases} u = fhan(x_1, x_2, r, h) \\ d = rh;\ d_0 = hd \\ y = x_1 + hx_2 \\ a_0 = \sqrt{d^2 + 8r|y|} \\ T = \begin{cases} x_2 + \frac{(a_0 - d)}{2}\mathrm{sign}(y), |y| > h^2r \\ x_2 + y/h, |y| \leq h^2r \end{cases} \\ fhan = -\begin{cases} r\mathrm{sign}(T), |T| > d \\ r\frac{T}{d}, |T| \leq d \end{cases} \end{cases} \qquad (13)$$

III. CONVERGENCE ANALYSIS

The main purpose of this section is to rigorously analyse the convergence of the DTOC algorithm in (11) for system (1) by demonstrating the state convergence trajectories. The main result is stated as follows.

For system (1) and the determined control signal sequence, $u(0), u(1), ..., u(k)$ in (11), any initial state point $M(x_{10}, x_{20})$ can converge to the origin in a minimum and finite number of steps, subject to the constraint that $|u(k)| \leq r$. That is, there exists $u(k^*)$, $|u(k)| \leq r$, such that $k^* = \min\{k|x(k) = 0\}$.

Before presenting the convergence analysis on this DTOC algorithm, we need to figure out whether isochronic region for any initial condition is unique or not. In other words, we have to show the monotonic characteristic of IR boundaries to clarify that any initial condition belongs to only one IR. In order to show this, equation in (9) is introduced, which partitions the whole phase plane in some manners (see Fig. 3).

Let

$$T(x_1, x_2, r, h) = x_2 + \frac{1}{2}(\sqrt{w} - hr)\mathrm{sign}(y)$$

where $\sqrt{w} = \sqrt{h^2r^2 + 8r|y|}$. We have

$$\begin{cases} \frac{\partial T}{\partial x_1} = \frac{2r}{\sqrt{w}} > 0 \\ \\ \frac{\partial T}{\partial x_2} = \frac{2hr}{\sqrt{w}} > 0, \end{cases} \qquad (14)$$

which implies that the boundaries of IR have the monotonic characteristic. According to (10), different values of h and r lead to different boundaries, that is,

$$\begin{cases} T(x_1, x_2, r, h) = c_1 \\ T(x_1, x_2, r, h) = c_2 \end{cases}$$

where $c_1 \neq c_2$. Therefore, there must exist a curve family $T(x_1, x_2, r, h) = c$ that divides the whole phase plane into different IRs (see Fig. 3), which clarifies that any initial condition can only belong to one IR.

Then convergence analysis of the $fhan$ algorithm can be carried out in the following several steps.

Step 1: Any initial state point $M(x_{10}(k), x_{20}(k))$ located below Γ_B^+ ($\tilde{\Gamma}^+$) or above Γ_A^+ ($\tilde{\Gamma}^-$) can converge to the region between Γ_B^+ and Γ_A^+.

Under this condition, the control algorithm takes on extreme value according the $fhan$ algorithm, that is,

$$u(k) = -r\text{sign}(s(k)) \qquad (15)$$

where $s(k) = x_1 + \frac{x_2|x_2|}{2r} + \frac{1}{2}hx_2$ is the curve Γ_A. Without loss of generality, we consider the initial state point $M(x_1(0), x_2(0))$ (denoted as $M(x_1, x_2)$ for simplicity) located above Γ_A^+ on the right side of phase plane, where exists $s(k) > 0$. The following Lyapunov function is constructed

$$\begin{aligned} \triangle s(k) &= s(k+1) - s(k) \\ &= hx_2(k) - \frac{1}{2}h^2r - h(x_2(k) - \frac{1}{2}hr)\text{sign}(x_2(k)) \\ &= h(x_2(k) - |x_2(k)|) - \frac{1}{2}h^2r(1 - \text{sign}(x_2(k))) \leq 0 \end{aligned}$$
$$(16)$$

There are two possible cases for the value of $\triangle s(k)$.

(1) If $x_2(k) > 0$, then $\triangle s(k) = 0$.

According to (11), the initial state $x_2(k)$ will keep decreasing until it arrives at Γ_A. There exists $x_2(k+1) = x_2(k) - hr$, that is, $x_2(k) = x_2(0) - khr$. Hence there exists a positive constant $k_0 = \frac{x_2(0)}{hr}$ that can make $x_2(k) < 0$ when $k > k_0$. Therefore, any initial state located above Γ_A on upper phase plane can be driven to lower phase plane where $x_2(k) < 0$.

(2) If $x_2(k) < 0$, then $\triangle s(k) = -2h|x_2(k)| - h^2r < -h^2r < 0$.

When $s(k) > 0$, there exists $s(k+1) - s(k) < -h^2r$, that is, $s(k) < s(0) - kh^2r$. Clearly there is a positive constant $k_1 = \frac{s(0)}{h^2r}$ that guarantees $s(k) < 0$ when $k > k_1$.

Similar conclusion can be obtained when the initial state $M(x_1(k), x_2(k))$ is located below Γ_B^+. The above statement manifests that any initial state $M(x_1, x_2)$ located below Γ_B^+ or above Γ_A^+ can converge to the region between Γ_B^+ and Γ_A^+ (see Fig. 4).

Step 2: Any initial state point $M(x_1, x_2)$ located inside the IR between Γ_B^+ and Γ_A^+ and beyond $G(2)$ cannot step out of this region inside which the state converges to $G(2)$.
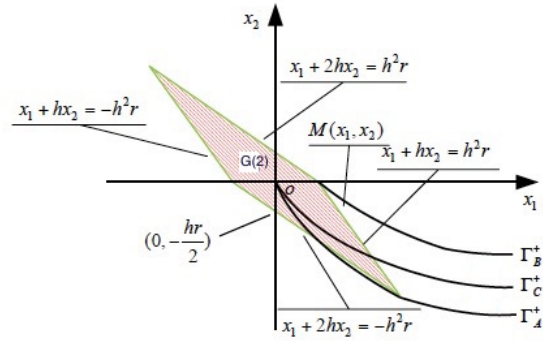

Fig. 4. Illustration of state trajectory when initial state is located above Γ_B^+ or below Γ_A^+.

Under this condition, there exists $T(x_1, x_2, r, h) \leq hr$, and the control algorithm takes on $u = -\frac{T(x_1, x_2, r, h)}{h}$. According to (9), we have

$$\begin{cases} T(k) = x_2(k) + \frac{(\sqrt{h^2r^2 + 8r|y(k)|} - hr)\text{sign}(y(k))}{2} \\ T(k+1) = x_2(k+1) + \frac{(\sqrt{h^2r^2 + 8r|y(k+1)|} - hr)\text{sign}(y(k+1))}{2} \end{cases}$$

where $y(k) = x_1(k) + hx_2(k) = x_1(k+1)$ and $y(k+1) = x_1(k+1) + hx_2(k+1)$. Further, we have

$$\begin{aligned} \triangledown T(k) &= T(k+1) - T(k) \\ &= x_2(k+1) + \frac{(\sqrt{h^2r^2 + 8r|y(k+1)|} - hr)}{2}\text{sign}(y(k+1)) \\ &\quad - x_2(k) - \frac{(\sqrt{h^2r^2 + 8r|y(k)|} - hr)}{2}\text{sign}(y(k)) \\ &= [x_2(k+1) - x_2(k)] + \frac{4r[y(k+1) - y(k)]}{\sqrt{w(k)} + \sqrt{w(k+1)}} \\ &= hu(k) + \frac{4hr[x_2(k) + hu(k)]}{\sqrt{w(k)} + \sqrt{w(k+1)}} \end{aligned}$$
$$(17)$$

where $\sqrt{w(k)}$ is the same as mentioned earlier.

Setting $Q(k) = \sqrt{w(k)} + \sqrt{w(k+1)}$, we have

$$\begin{aligned} T(k+1) &= T(k) + hu(k) + \frac{4hr[x_2(k) + hu(k)]}{Q(k)} \\ &= \frac{4hr}{Q(k)}[x_2(k) - T(k)] \\ &= -hr\Big[\frac{2}{1 + \sqrt{\frac{w(k+1)}{w(k)}}} - \frac{2hr}{Q(k)}\Big]\text{sign}(y(k)) \qquad (18) \\ &= -hr\Big[\frac{\sqrt{w(k)} - hr}{\frac{\sqrt{w(k)} + \sqrt{w(k+1)}}{2}}\Big]\text{sign}(y(k)) \end{aligned}$$

Without loss of generality, the condition of $y(k) > 0$ is taken into consideration. If there exists

$$0 < \frac{\sqrt{w(k)} - hr}{\frac{\sqrt{w(k)} + \sqrt{w(k+1)}}{2}} < 1, \qquad (19)$$

then we have $|T(k+1)| < hr$ (Note that the condition $|T(k)| < hr$ holds at the beginning), which means any initial state point $M(x_1, x_2)$ located inside the IR between
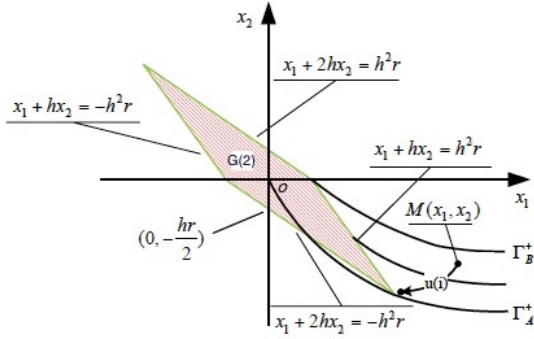
Fig. 5. Illustration of state trajectory when initial state is located inside IR between Γ_B^+ and Γ_A^+ and beyond $G(2)$.

Γ_B^+ and Γ_A^+ and beyond $G(2)$ cannot step out of this region. Meanwhile, because there exist $\nabla x_2(k) = hu(k)$ and $u = -\frac{T(x_1,x_2,r,h)}{h}$, $|x_2(k)|$ will decrease monotonously, meaning that the initial state point $M(x_1, x_2)$ will converge to $G(2)$.

Now we need to analyse inequality (19). Apparently, $0 < \frac{\sqrt{w(k)}-hr}{\frac{\sqrt{w(k)}+\sqrt{w(k+1)}}{2}}$ holds since $\sqrt{w} = \sqrt{h^2r^2 + 8r|y|} > hr$. To show that $\frac{\sqrt{w(k)}-hr}{\frac{\sqrt{w(k)}+\sqrt{w(k+1)}}{2}} < 1$, we have

$$\frac{\sqrt{w(k)} - hr}{\frac{\sqrt{w(k)}+\sqrt{w(k+1)}}{2}} < 1$$
$$\Longleftrightarrow \sqrt{w(k)} < 2hr + \sqrt{w(k+1)}$$
$$\Longleftrightarrow w(k) < 4h^2r^2 + 4hr\sqrt{w(k+1)} + w(k+1)$$
$$\Longleftrightarrow x_2(k+1) + \frac{1}{2}hr + \frac{1}{2}\sqrt{w(k+1)} > 0$$
$$\Longleftrightarrow x_2(k+1) + \frac{1}{2}(\sqrt{w(k+1)} - hr)\text{sign}(y(k+1)) > -hr$$
$$\Longleftrightarrow T(k+1) > -hr$$
$$\tag{20}$$

Based on the above analysis, the condition in (19) holds. Thus, any initial state point $M(x_1, x_2)$ located inside the IR between Γ_B^+ and Γ_A^+ and beyond $G(2)$ cannot step out of this region and the state converges to $G(2)$ (see Fig. 5).

Step 3: Any initial state point $M(x_1, x_2)$ located inside $G(2)$ can converge to the origin with at most two steps.

When the initial state point $M(x_1, x_2)$ is inside $G(2)$, there exists

$$u(0) = -\frac{x_1(0) + 2hx_2(0)}{h^2} = \frac{x_2(0) + y(0)/h}{h} \tag{21}$$

Further, we have

$$x(1) = \begin{bmatrix} x_1(0) + hx_2(0) \\ x_2(0) + hu(0) \end{bmatrix} = \begin{bmatrix} y(0) \\ -y(0)/h \end{bmatrix} \in G(1) \tag{22}$$

Therefore, any initial condition $M(x_1, x_2) \in G(2)$ will be driven into $G(1)$ and then is back to the origin.

The above analysis in a few steps shows the convergence performance of $fhan$ algorithm.
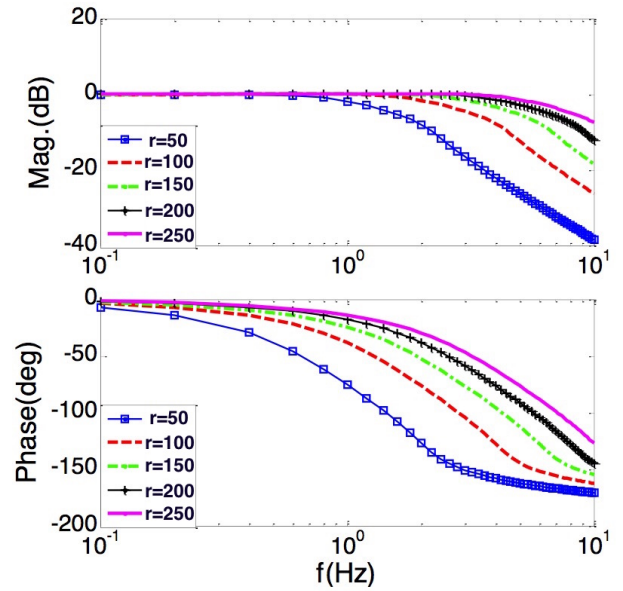

Fig. 6. Frequency-domain characteristics of tracking output x_1.

IV. FREQUENCY-DOMAIN CHARACTERISTICS ANALYSIS

According to the $fhan$ algorithm, with a given reference signal sequence $v(k), k = 0, 1, 2, ...$ corrupted with a random noise, the following TD can be constructed

$$\begin{cases} u(k) = fhan(x_1(k) - v(k), x_2(k), r, c_0h) \\ x_1(k+1) = x_1(k) + hx_2(k) \\ x_2(k+1) = x_2(k) + hu(k), |u(k)| \leq r, k = 0, 1, 2, ... \end{cases} \tag{23}$$

where v is the input signal to be differentiated, x_1 is the desired trajectory, x_2 is its derivative and c_0 is the filtering factor. It is utilized to provide the fastest tracking of $v(k)$ and its differentiation estimation subject to the acceleration limit of r.

The tuning parameter r in (23) plays an essential role in deciding the speed and precision of signal tracking and differentiation estimation. Specifically, the $fhan$ algorithm based TD can track the input and estimate the corresponding differentiation with arbitrary precision when r tends to infinity. Under practical limitations, r can only regulate within a certain bound. This may lead to high-frequency attenuation with a selected r once the frequency of the input signals exceeds a certain range. Meanwhile, the TD is insensitive to the noises, which enables its good filtering ability.

In this section, we shall analyse the characteristics of the output signals of the TD in frequency-domain by means of the frequency-sweep. We assume that the frequency of input signals have a range of $[0.1Hz, \ 10Hz]$. The initial condition is $P(x_1, x_2) = P(1, -1)$ and the filtering factor $c_0 = 3$. The amplitude-frequency and phase-frequency response curves under different values of the r are shown in Fig. 6 and Fig. 7, respectively.

From Fig. 6, the frequency-domain characteristics of output x_1 approximates a low-pass filter. When the frequency of input signals is lower than the turnover frequency, the amplitude-frequency characteristics is similar to a straight line parallel to
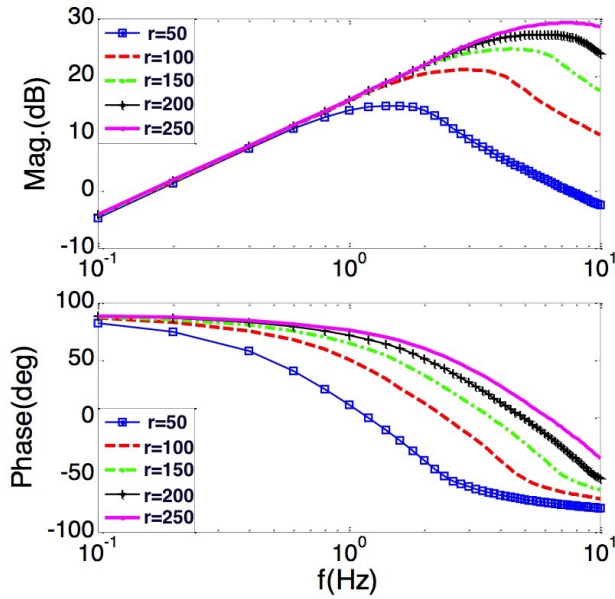
Fig. 7. Frequency-domain characteristics of differentiation estimation x_2.

the x-axis. Meanwhile, the phase-frequency response change gradually with a small phase delay. However, when the frequency of input signals is greater than the turnover frequency, compared with input signals, the amplitude attenuation and phase delay are apparent.

From Fig. 7, we see that the frequency-domain characteristics of output x_2 (differentiation estimation) approximates the bandpass filter. When the frequency of input signals is lower than the turnover frequency, the amplitude of output x_2 increases as the frequency goes up, and the phase lead remains over $90°$. Similarly, the amplitude attenuation and phase delay are apparent when the frequency of input signals is greater than the turnover frequency.

Further, from Figs. 6 and 7, we see that the turnover frequency of the proposed TD rises as the tuning parameter r increases. This represents that a relatively bigger r enables the proposed TD track a higher frequency of input signals and enhances the estimation of the corresponding differentiation. However, the ability of restraining the noise meanwhile is reduced. In practice, a proper value of the parameter r can be selected accordingly to speed up or slow down the transient profile.

V. CASE STUDIES

A. Simulation Comparisons

In this subsection, we give some numerical simulations to compare the $fhan$ based tracking differentiator (denoted as **D4**) with other differentiators.

D1: Nonlinear tracking differentiator with high speed in the whole course [8]:

$$\begin{cases} \dot{x}_1 = x_2 \\ \dot{x}_2 = R^2(-a_0(x_1 - v(t)) - a_1(x_1 - \\ \quad v(t))^{m/n} - b_0 \frac{x_2}{R} - b_1 (\frac{x_2}{R})^{m/n}) \end{cases}$$
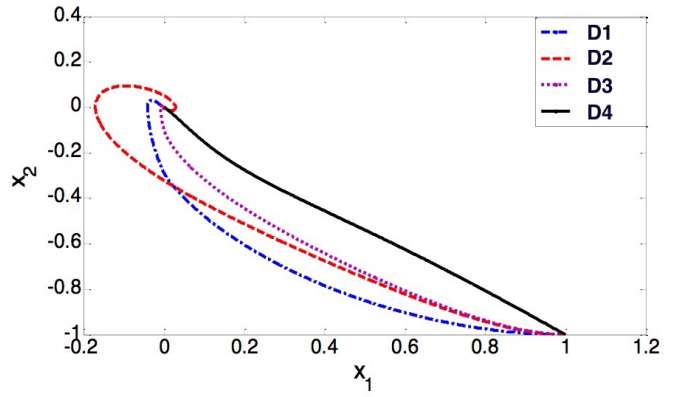

Fig. 8. The state trajectories of four different differentiators.

where the parameters $R, a_0, a_1, b_0, b_1 > 0$, $m, n > 0$ are odd numbers.

D2: Linear tracking differentiator [11]

$$\begin{cases} \dot{x}_1 = x_2 \\ \dot{x}_2 = R_1^2(-(x_1 - v(t)) - \frac{x_2}{R_1}) \end{cases}$$

where R_1 is a tuning parameter.

D3: Robust exact differentiator using the sliding-mode technique [4].

$$\begin{cases} \dot{x}_1 = x_2 - \alpha|x_1 - v|^{0.5}\text{sign}(x_1 - v), \\ \dot{x}_2 = -\beta\text{sign}(x_1 - v) \end{cases}$$

where α and β are two tuning parameters.

The Matlab program of the Euler method is adopted in the investigation. We choose the same zero initial condition $(-1, 1)$, the sampling period $h = 0.0001$, and $v(t) = 0$ in all simulations. All parameters are given by the trial and error method, where $\alpha = 2$ and $\beta = 6$ for **D3**. The state trajectories of these four differentiators are plotted in Fig. 8.

As can be seen in Fig. 8, with the same initial condition and input, the $fhan$ based TD is the fastest one among the four differentiators to drive the initial condition into the origin. With the same simulation environment, we further investigate signal-tracking and differentiation acquisition by the four differentiators in Fig. 9. The results show that again the $fhan$ based TD has the fastest convergence speed without having an overshoot problem.

B. Experiments of an application in maglev train

In a maglev train, the active suspension control must be applied to ensure the stability of levitation [24], [25]. The schematic diagram of a suspension control system is shown in Fig. 10.

Installed at electromagnet, the gap sensor is applied to measure the gap (z) between the upper surface of the electromagnet and the lower surface of the track; while the acceleration sensor is used to acquire the vertical motion acceleration (a) of the electromagnet. Voltage (U_I, U_{II}), current (I_I, I_{II}) and temperature (T) sensors are installed inside the the controller. In practice, the gap signals (z) and its corresponding speed signals ($\dot{z}$) are vital to construct suspension controller. The
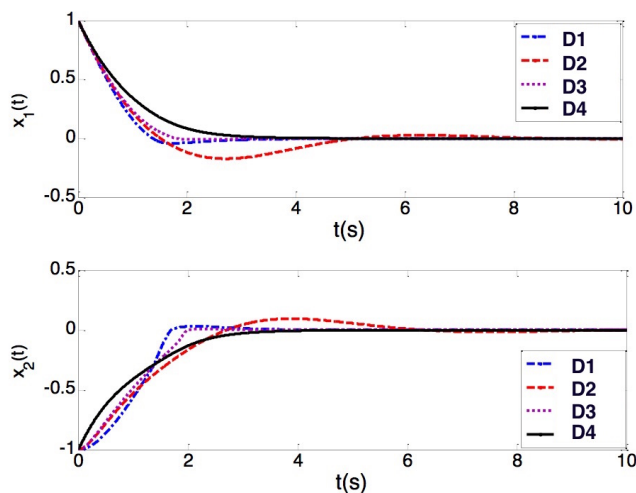
Fig. 9. Comparisons of signal-tracking x_1 and differentiation acquisition x_2 among four different differentiators.
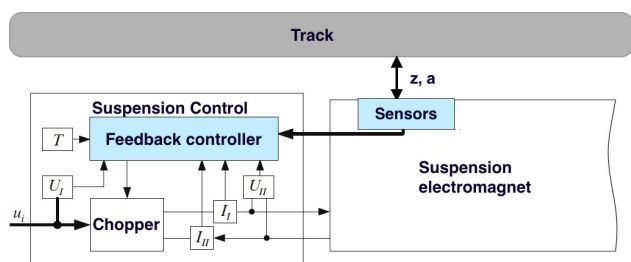

Fig. 10. A single-point suspension control system.

gap signals, however, are prone to be corrupted by noises. This makes speed signals obtained from some typical differentiators be quite sensitive to the noises. The acceleration sensor is therefore applied to acquire speed signals by integrator. The expensive accelerometer however has a relatively high chance to fail because of the harsh operating conditions. There is an urgent need to adopt an effective method to extract speed signals from gap sensors.

As shown in Fig. 11, the real-time field data reflecting the gap between the electromagnet and the track is collected by a gap sensor (JXCF-TL-KD-02-N), and then is processed by the FPGA inside control panel. The sampling period of the gap sensor is 40 kHz and the FPGA is with the speed of 50 MHz. Specifically, the gap data is collected from the static suspension scenario where the maglev train keeps in stable suspension state and has no horizontal motion. In this scenario, the suspension gap is 8 mm. To clearly demonstrate the comparisons on differentiation acquisition among different differentiator, we let the 8 mm correspond to 0 point in y-axis. Note that the steady-state error within $\pm$ 0.3 mm meets the requirements of practical maglve engineering.

The $fhan$ based TD was tested and experimentally compared with the classical differentiator (see [11]) applied in maglev engineering now. To evaluate the $fhan$ algorithm, all involved parameters of both differentiators are selected by the method of trial and error. Therein, the parameter
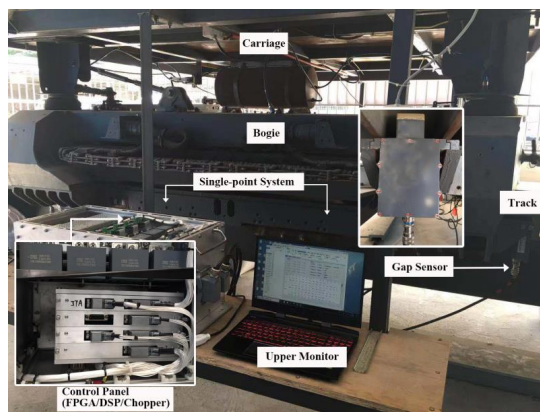

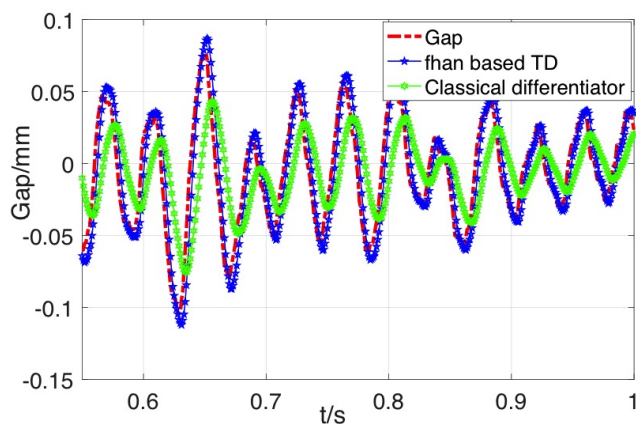Fig. 11. Experimental platform of a maglev bogie with suspension control systems.
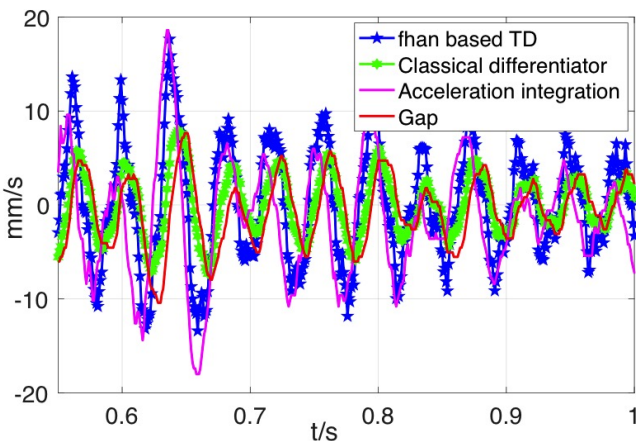

Fig. 12. Gap tracking filtering.

Fig. 13. Speed estimation.

$r = 3000$ and $c_0 = 5$ are adopted for $fhan$ based TD, and the two time constants in the classical differentiator are selected as $\tau_1 = 0.002$ and $\tau_1 = 0.0025$, respectively. The signal processing comparison results including gap signal-tracking filtering and speed acquisition are shown in Figs. 12 and 13, respectively.

The results show that the $fhan$ based TD, compared with

the classical differentiator, can produce better signal-tracking filtering and speed acquisition that meet the requirements of practical maglve engineering. This indicates that $fhan$ based TD is possible to complement or even replace the acceleration sensor in the future maglev train systems to reduce the costs and improve the reliability of suspension systems.

VI. CONCLUSION

The DTOC algorithm ($fhan$) resolves the long standing issue of chattering in the control signals and therefore, provides a practical solution better than the well known bang-bang control. The convergence analysis of the DTOC-TD has been investigated in this paper by adopting Lyapunov functions. The proof guarantees that for any given initial state, the system can converge to the steady state within a finite number of steps, which not only makes its applications technically sound, but also provides the theoretical foundation of ADRC. Comparison simulation results showed that this DTOC-TD has better performance in signal-tracking filtering and differentiation acquisition than the other existing ones, in particular, in dynamic process and chattering alleviation. The experiments carried out on the gap sensor in maglev train verified that the DTOC-TD is effective in filtering and speed acquisition, which also implies its great potentials in other industrial applications. Future work includes the phase delay compensation algorithm, and developing the higher-order TD based on higher-order DTOC algorithms.

REFERENCES

[1] J. Han, "From PID to active disturbance rejection control," *IEEE Trans. Ind. Electron.*, vol. 56, no. 3, pp.900-906, 2009.

[2] H. Ríos, E. Punta, and L. Fridman, "Fault detection and isolation for nonlinear non-affine uncertain systems via sliding-mode techniques," *Int. J. Control*, vol. 90, no. 2, pp. 218-230, 2017.

[3] C. Vázquez, S. Aranovskiy, L. Freidovich, and L. Fridman, "Time-varying gain differentiator: A mobile hydraulic system case study," *IEEE Trans. Contr. Syst. T.*, vol. 24, no. 5, pp. 1740-1750, 2016.

[4] A. Levant, "Robust exact differentiation via sliding mode technique," *Automatica*, vol. 34, no. 3, pp. 379-384, 1998.

[5] A. Levant and X. Yu, "Sliding-mode-based differentiation and filtering," *IEEE Trans. Autom. Control*, vol. 63, no. 9, pp. 3061-3067, 2018.

[6] A. Dabroom and H. Khalil, "Output feedback sampled-data control of nonlinear systems using high-gain observers," *IEEE Trans. Autom. Control*, vol. 46, no. 11, pp. 1712-1725, 2001.

[7] S. Ibrir, "Linear time-derivative trackers," *Automatica*, vol. 40, no. 3, pp. 397-405, 2004.

[8] X. Wang, Z. Chen, and G. Yang, "Finite-time-convergent differentiator based on singular perturbation technique," *IEEE Trans. Autom. Control*, vol. 52, no. 9, pp. 1731-1737, 2007.

[9] Y. Feng, J. Zheng, X. Yu, and N. Truong, "Hybrid terminal sliding-mode observer design method for a permanent-magnet synchronous motor control system," *IEEE Trans. Ind. Electron.*, vol. 56, no. 9, pp. 3424-3431, 2009.

[10] W. Chen, J. Yang, L. Guo, and S. Li, "Disturbance-observer-based control and related methods-An overview," *IEEE Trans. Ind. Electron.*, vol. 63, no. 2, pp. 1083-1095, 2015.

[11] J. Han, *Active Disturbance Rejection Control Technique-The Technique for Estimating and Compensating the Uncertainties*, Beijing, China: Nat. Defense Ind. Press, 2008.

[12] J. Li, Y. Xia, X. Qi, and Z. Gao, "On the necessity, scheme, and basis of the linear-nonlinear switching in active disturbance rejection control," *IEEE Trans. Ind. Electron.*, vol. 64, no. 2, pp. 1425-1435, 2016.

[13] L. Bonifacius, K. Pieper, and B. Vexler, B, "Error estimates for space-time discretization of parabolic time-optimal control problems with bang-bang controls," *SIAM J Control Optim.*, vol. 57, no. 3, pp. 1730-1756, 2019.

[14] W. Newman, "Robust near time-optimal control," *IEEE Trans. Autom. Control*, vol. 35, no. 7, pp. 841-844, 1990.

[15] R. Bertrand and R. Epenoy, "New smoothing techniques for solving bang-bang optimal control problems-numerical results and statistical interpretation," *Optim Contr Appl Met.*, vol. 23, no. 4, pp. 171-197, 2002.

[16] J. Han and L. Yuan, "The Discrete Form of the Tracking Differentiator," *Syst. Sci. Math.*, vol. 19, no. 3, pp. 268-273, 1999. (In Chinese)

[17] B. Guo and Z. Zhao, *Active disturbance rejection control for nonlinear systems: An introduction*, John Wiley & Sons. 2016.

[18] W. Xue, Y. Huang, and X. Yang, "What kinds of system can be used as tracking-differentiator," *In Proceedings of the 29th Chinese Control Conference*, pp. 6113-6120, July 2010.

[19] B. Guo and Z. Zhao, "On convergence of tracking differentiator," *Int. J. Control*, vol. 84, no. 4, pp. 693-701, 2011.

[20] Z. Gao, "On discrete time optimal control: A closed-form solution," *In Proceedings of the 2004 American Control Conference*, vol. 1, pp. 52-58, June 2004.

[21] N. Zhang, W. Gai, G. Zhang, and J. Zhang, "An active disturbance rejection control guidance law based collision avoidance for unmanned aerial vehicles," *Aerospace Science and Technology*, vol. 77, pp. 658-669, 2018.

[22] H. Wu and J. Huang, "Control of induction motor drive based on ADRC and inertia estimation," *In 2019 IEEE International Electric Machines & Drives Conference (IEMDC)*, pp. 1607-1612, May 2019.

[23] Q. Dong, Y. Liu, Y. Zhang, S. Gao, and T. Chen, "Improved ADRC with ILC control of a CCD-Based tracking loop for fast steering mirror system," *IEEE Photonics Journal*, vol. 10, no. 4, pp. 1-14, 2018.

[24] H. Lee, K. Kim, and J. Lee, "Review of maglev train technologies," *IEEE Trans. Magn.*, vol. 42, no. 7, pp. 1917-1925, 2006.

[25] Y. Sun, J. Xu, H. Qiang, and G. Lin, "Adaptive neural-fuzzy robust position control scheme for Maglev train systems with experimental verification," *IEEE Trans. Ind. Electron.*, 2019.